Anal. Chem. **2005,** *77,* 1088−1095

Ordered Silicon Nanocavity Arrays in Surface-Assisted Desorption/Ionization Mass Spectrometry

Nancy H. Finkel,† Brian G. Prevo,‡ Orlin D. Velev,‡ and Lin He*,†

Departments of Chemistry and Chemical Engineering, North Carolina State University, Raleigh, North Carolina 27695

We report here a simple method to generate ordered nanocavity arrays on a Si wafer and use it in surface-assisted laser desorption/ionization mass spectrometry (SALDI-MS). A close-packed SiO_2 nanosphere array was first deposited on a low-resistivity Si wafer using a convective self-assembly method. The nanoparticle array was then used as a mask in a reactive ion etching (RIE) process to selectively remove portions of the Si surface. Subsequent sonication removed those physically adsorbed SiO_2 nanoparticles and exposed an ordered nanocavity array underneath. The importance of this approach is its capability of systematically varying surface geometries to achieve desired features, which makes detailed studies of the impacts of surface features on the desorption/ionization mechanism feasible. We demonstrated that the in-plane width and out-of-plane depth of the cavities were adjustable by varying etching times, and the intercavity spacing was controllable by varying the number of particle layers deposited. MS detection of small peptides on these substrates showed comparable sensitivity to conventional porous Si substrates (DIOS, desorption/ionization on porous silicon). The desorption and ionization efficiency of these roughened surfaces exhibited a nonmonotonic relationship to the increased total surface area. Several possible factors contributing to the observed phenomenon are speculated upon. The application of this arrayed surface in metabolite detection of *Arabidopsis thaliana* root extracts is also demonstrated.

The matrixes used in matrix-assisted laser desorption/ionization (MALDI), a group of small organic molecules to facilitate the desorption of analytes, have played a paramount role in the success of MALDI mass spectrometry (MS) in life science.[1−5] As energy mediators, MALDI matrixes effectively transfer absorbed photon energy from an irradiation source to the surrounding sample molecules.[4−6] However, the introduction of background ions at the low-mass region from these matrixes has limited MALDI applications in the field of small-molecule detection. One alternative technique of using surface-assisted laser desorption/ionization (SALDI) substrates, a special subgroup of desorption facilitators of inorganic particles or surfaces, has thus drawn considerable attention.[2,3,7−12] With low atomic masses and good stability during desorption, these substrates reduce the overwhelming background at the low-mass region that is often observed from conventional MALDI matrix fragmentation. Tanaka et al. have pioneered the research in this field by mixing glycerol solution with fine cobalt powders.[2] These 30-nm cobalt particles absorbed light with high efficiency, resulting in a significantly increased local temperature. The heat was then transferred to the surrounding glycerol/analyte solution, and the analyte molecules were brought into the gas phase, where they were detected as ions. Sunner and his group have expanded the concept to micrometer-sized graphite particles and other inorganic materials as the matrixes and have been actively engaged in understanding the SALDI mechanism.[13−15] Along a similar line, a variety of inorganic materials, such as W, Ag, ZnO, TiO_2, Si, SiO_2 nanoparticles, active carbon, and carbon nanotubes, have all been evaluated as SALDI matrixes with different degrees of success.[7,16−21]

* Corresponding author. Fax: 919-515-5079. E-mail: lin_he@ncsu.edu.
† Department of Chemistry.
‡ Department of Chemical Engineering.

(1) Aebersold, R.; Mann, M. *Nature* **2003**, *422*, 198−207.
(2) Tanaka, K.; Waki, H.; Ido, Y.; Akita, S.; Yoshida, Y.; Yoshida, T. *Rapid Commun. Mass Spectrom.* **1988**, *2*, 151−153.
(3) Hillenkamp, F.; Bahr, U.; Karas, M.; Spengler, B. *Scanning Microsc., Suppl.* **1987**, *1*, 33−39.
(4) Zenobi, R.; Breuker, K.; Knochenmuss, R.; Lehmann, E.; Stevenson, E. *Adv. Mass Spectrom.* **2001**, *15*, 143−149.
(5) Menzel, C.; Dreisewerd, K.; Berkenkamp, S.; Hillenkamp, F. *Int. J. Mass Spectrom.* **2001**, *207*, 73−96.
(6) Bencsura, A.; Navale, V.; Sadeghi, M.; Vertes, A. *Rapid Commun. Mass Spectrom.* **1997**, *11*, 679−682.
(7) Dale, M. J.; Knochenmuss, R.; Zenobi, R. *Anal. Chem.* **1996**, *68*, 3321−3329.
(8) Chen, Y.-C.; Shiea, J.; Sunner, J. *J. Chromatogr., A* **1998**, *826*, 77−86.
(9) Schuerenberg, M.; Dreisewerd, K.; Hillenkamp, F. *Anal. Chem.* **1999**, *71*, 221−229.
(10) Wei, J.; Buriak, J. M.; Siuzdak, G. *Nature* **1999**, *399*, 243−246.
(11) Bhattacharya, S. H.; Raiford, T. J.; Murray, K. K. *Anal. Chem.* **2002**, *74*, 2228−2231.
(12) Cuiffi, J. D.; Hayes, D. J.; Fonash, S. J.; Brown, K. N.; Jones, A. D. *Anal. Chem.* **2001**, *73*, 1292−1295.
(13) Sunner, J.; Dratz, E.; Chen, Y.-C. *Anal. Chem.* **1995**, *67*, 4335−4342.
(14) Kraft, P.; Alimpiev, S.; Dratz, E.; Sunner, J. *J. Am. Soc. Mass Spectrom.* **1998**, *9*, 912−924.
(15) Alimpiev, S.; Nikiforov, S.; Karavanskii, V.; Minton, T.; Sunner, J. *J. Chem. Phys.* **2001**, *115*, 1891−1901.
(16) Han, M.; Sunner, J. *J. Am. Soc. Mass Spectrom.* **2000**, *11*, 644−649.
(17) Kinumi, T.; Saisu, T.; Takayama, M.; Niwa, H. *J. Mass Spectrom.* **2000**, *35*, 417−422.
(18) Xu, S.; Li, Y.; Zou, H.; Qiu, J.; Guo, Z.; Guo, B. *Anal. Chem.* **2003**, *75*, 6191−6195.
(19) Armstrong, D. W.; Zhang, L.-K.; He, L.; Gross, M. L. *Anal. Chem.* **2001**, *73*, 3679−3686.
(20) Kim, J.; Kang, W. *Bull. Korean Chem. Soc.* **2000**, *21*, 401−404.

10.1021/ac048645v CCC: $30.25
Published on Web 01/20/2005

The most prominent example in this class of approaches was reported by Siuzdak and co-workers, in which a porous silicon surface was used in desorption/ionization on porous silicon (DIOS), a particle-free version of SALDI.[10,22−24] Small molecules including pharmaceuticals, peptides, polymers, and protein proteolytic products have all been detected with impressive sensitivities using this kind of substrate.[11, 25−28]

Encouraged by the success of DIOS substrates, various methods have been reported to generate porous Si structures for MS applications, including the use of conventional electrochemical etching,[10,22] plasma-enhanced chemical vapor deposition (PECVD),[12] hyperthermal reactive atom etching,[15] and direct nanoparticle mixing,[21] etc. To prepare a high-performance substrate reproducibily using any of these methods is, however, not trivial. Most methods yield a broad range of pore sizes, depths, and densities on the same surface that often causes spot-to-spot and batch-to-batch variations in SALDI performance. Developing methods to reproducibly generate porous Si substrates with optimal porosity and thickness is thus critical to broader applications of SALDI. Furthermore, the complexity of the analyte desorption and ionization process makes it a great challenge for both theorists and experimentalists to elucidate the exact energy- and proton-transferring pathways in the laser-based desorption/ionization process. The capability to systematically vary surface features and independently fine-tune one influential component at a time is therefore desirable for the in-depth understanding of surface morphological contributions to desorption and ionization of absorbed analytes.

Running in parallel to the rapid development of MS techniques, material scientists and engineers are perfecting various methods to construct large-scale two-dimensional and three-dimensional nanostructures with high precision and great flexibility.[29−32] Both top-down lithographic patterning techniques and bottom-up self-assembly processes have been demonstrated for the fabrication of functional nanoscale structures and devices in the literature.[33−36] On the basis of convective self-assembly, the groups of Velev,[37,38] Van Duyne,[39,40] and others have reported successful deposition of large areas of hexagonally packed two-dimensional crystals of nanospheres on solid substrates.[41−43] Such crystals have also been used as masks for the fabrication of ordered cavity arrays when coupled with reactive ion etching (RIE).[44−46]

In this paper, we described such nanosphere lithography-coupled RIE method to be used to generate ordered nanostructures on a Si wafer. The method is simple yet reproducible and can find great applications in controllable fabrication of efficient SALDI substrates. Preliminary experiments illustrate the presence of the correlation between surface features and the observed MS desorption/ionization efficiency. The suitability of the prepared surface for the detection of small peptides in the mass range of 200−1500 m/z is examined, and its application in metabolite detection is demonstrated.

EXPERIMENTAL SECTION

Materials. SiO_2 beads of 330-nm diameter were purchased from Bangs Lab (Fisher, IN) and used as received (10% weight content). Phosphorus-doped (100) single-crystalline silicon wafer at 0.5−2 Ω/cm was purchased from Silicon Sense, Inc. (Nashua, NH). The wafers were stored under vacuum until needed. HF (49%), H_2SO_4, H_2O_2 (30%), CH_3OH (HPLC grade), and H_2O (HPLC grade) were purchased from Fisher Scientific (Pittsburgh, PA). CH_3CH_2OH was purchased from Aaper Alcohol (Shelbyville, KY). Angiotensin I, bradykinin, Ala-Leu-Ala-Leu, Val-Met, and trifluoric acid (TFA) were purchased from Sigma Aldrich (St. Louis, MO). DI H_2O of 18 MΩ (Millipore, PO) was used throughout the experiments.

Surface Preparation. The Si wafer was cut into approximately 2-in.^{2} workable chips and dipped in 5% HF/CH_3CH_2OH for 2 min to remove the oxide layer prior to the use. It was then purposely oxidized with ozone for 10 min in an ultraviolet/ozone (UVO) chamber (Model 42, Jelight Co., Inc.) and/or further oxidized and cleaned by soaking in a piranha solution (3:1 H_2SO_4/H_2O_2 [*Caution! Hazardous and corrosive chemicals*]) for 2 h. After being washed with copious amounts of DI H_2O, the wafer was dried in a baking oven at 60−70 °C for 2 h. The microscope glass slides used as spreaders in convective assembly were also cleaned and dried, following the same procedure. SiO_2 beads were spread on the Si wafer using a home-built convective assembly device, as described elsewhere.[38] During the deposition, 10−15 μL of SiO_2 bead suspension was spread at a rate of 20−45 μm/s.

(21) Zhang, Q.; Zou, H.; Guo, Z.; Zhang, Q.; Chen, X.; Ni, J. *Rapid Commun. Mass Spectrom.* **2001**, *15*, 217−223.
(22) Go, E. P.; Prenni, J. E.; Wei, J.; Jones, A.; Hall, S. C.; Witkowska, H. E.; Shen, Z.; Siuzdak, G. *Anal. Chem.* **2003**, *75*, 2504−2506.
(23) Shen, Z.; Thomas, J. J.; Averbuj, C.; Broo, K. M.; Engelhard, M.; Crowell, J. E.; Finn, M. G.; Siuzdak, G. *Anal. Chem.* **2001**, *73*, 612−619.
(24) Trauger, S. A.; Go, E. P.; Shen, Z.; Apon, J. V.; Compton, B. J.; Bouvier, E. S. P.; Finn, M. G.; Siuzdak, G. *Anal. Chem.* **2004**, *76*, 4484−4489.
(25) Kruse, R. A.; Rubakhin, S. S.; Romanova, E. V.; Bohn, P. W.; Sweedler, J. V. *J. Mass Spectrom.* **2001**, *36*, 1317−1322.
(26) Thomas, J. J.; Shen, Z.; Crowell, J. E.; Finn, M. G.; Siuzdak, G. *Proc. Natl. Acad. Sci. U.S.A.* **2001**, *98*, 4932−4937.
(27) Arakawa, R.; Shimomae, Y.; Morikawa, H.; Ohara, K.; Okuno, S. *J. Mass Spectrom.* **2004**, *39*, 961−965.
(28) Wall, D. B.; Finch, J. W.; Cohen, S. A. *Rapid Commun. Mass Spectrom.* **2004**, *18*, 1403−1406.
(29) Zhao, X.-M.; Xia, Y.; Whitesides, G. M. *J. Mater. Chem.* **1997**, *7*, 1069−1074.
(30) Seebohm, G.; Craighead, H. G. *Electron. Mater. Ser.* **2000**, *6*, 97−138.
(31) Xia, Y.; Whitesides, G. M. *Annu. Rev. Mater. Sci.* **1998**, *28*, 153−184.
(32) Kraemer, S.; Fuierer, R. R.; Gorman, C. B. *Chem. Rev.* **2003**, *103*, 4367−4418.
(33) Kato, T.; Yabuuchi, K.; Sugawara, A.; Kishimoto, K. *Materia* **2003**, *42*, 453−456.
(34) Schmidt, O. G.; Deneke, C.; Nakamura, Y.; Zapf-Gottwick, R.; Mueller, C.; Jin-Phillipp, N. Y. *Adv. Solid State Phys.* **2002**, *42*, 231−240.
(35) Jiang, P.; Bertone, J. F.; Hwang, K. S.; Colvin, V. L. *Chem. Mater.* **1999**, *11*, 2132−2140.
(36) Dimitrov, A. S.; Nagayama, K. *Chem. Phys. Lett.* **1995**, *243*, 462−468.
(37) Velev, O. D.; Jede, T. A.; Lobo, R. F.; Lenhoff, A. M. *Nature* **1997**, *389*, 447−448.
(38) Prevo, B. G.; Velev, O. D. *Langmuir* **2004**, *20*, 2099−2107.
(39) Haynes, C. L.; Van Duyne, R. P. *J. Phys. Chem. B* **2001**, *105*, 5599−5611.
(40) Ormonde, A. D.; Hicks, E. C. M.; Castillo, J.; Van Duyne, R. P. *Langmuir* **2004**, *20*, 6927−6931.
(41) Dushkin, C. D.; Yoshimura, H.; Nagayama, K. *Chem. Phys. Lett.* **1993**, *204*, 455−459.
(42) Denkov, N. D.; Velev, O. D.; Kralchevsky, P. A.; Ivanov, I. B.; Yoshimura, H.; Nagayama, K. *Nature* **1993**, *361*.
(43) Denkov, N. D.; Velev, O. D.; Kralchevsky, P. A.; Ivanov, I. B.; Yoshimura, H.; Nagayama, K. *Langmuir* **1992**, *8*, 3183−3190.
(44) During our paper preparation, similar work from two groups has been published on using nanosphere lithography coupled-RIE to fabricate nanocavity arrays.[45,46]
(45) Choi, D.-G.; Yu, H. K.; Jang, S. G.; Yang, S.-M. *J. Am. Chem. Soc.* **2004**, *126*, 7019−7025.
(46) Whitney, A. V.; Myers, B. D.; Van Duyne, R. P. *Nano Lett.* **2004**, *4*, 1507−1511.

Polycrystalline arrays of SiO_2 nanoparticles were assembled as the thin wetting film evaporated by combination of convection, capillary forces, and free volume reduction. The resulting film was visually inspected for uniformity. The coated substrates were then stored in plastic Petri dishes to avoid contamination.

Reactive Ion Etching. A SemiGroup reactive ion etching (RIE) system 1000TP in the NCSU Nanofabrication Facility was used to transfer the ordered SiO_2 particle patterns onto the Si wafer. The radio frequency power used to generate plasma was set at 100 W. The chamber pressure was set to 50 mTorr. The RIE time was varied in the experiment from 0.5 to 5 min. A mixture of SF_6 and O_2 was used as the etching gas with gas flow rates at 15 and 5 cm^3(STP)/min, respectively. After RIE, the beads were removed via sonication in 10 mL of EtOH for 30 min. Surfaces were stored in EtOH in glass Petri dishes until needed. Traditional DIOS substrates were prepared using an electrochemical etching method, as described in the literature.[10,23]

Surface Characterization. A FEI XL30 SEM-FEG field emission scanning electron microscope (FE-SEM) was used to examine the surface features. The working voltage was 5 kV with a working distance of ~5 mm. Due to the difficulty of fine-tuning SEM magnification levels in our current instrument setup, the collected images were adjusted to the same scale using Adobe photoshop for comparison. Note that while the resolution of the images was changed due to this process, the geometry of the surface features was unaffected. The Si wafer was broken in the middle and attached to an aluminum block to examine the cross-section of the etched features. Approximately 20 cavities and posts from each surface were randomly chosen to measure the size distribution of surface features.

Plant Extract. Roots from smaller batches (10−15 plants/sample) of *Arabidopsis thaliana* (*A. thaliana*; ecotype Col-O) were pooled and flash-frozen in liquid N_2. The samples were then mixed with 200 μL of 80% MeOH and ground in a bead beater with 0.5-mm glass beads for 2 × 1 min with incubation on ice for 2 min in between. After being centrifuged twice at 15000*g* for 10 min at 40 °C in a microcentrifuge, the supernatant was stored at −20 °C until analysis.

Mass Spectrometry Analysis. Two analyte mixtures were used as the standards to evaluate the performance of nanocavity-arrayed Si substrates. One mixture included bradykinin (MW = 1060.6) and angiotensin I (MW = 1296.7), prepared at a concentration of 10 pmol/μL each. Val-Met (MW = 248.1) and Ala-Leu-Ala-Leu (MW = 386.3) were prepared at a concentration of 20 pmol/μL each in the second mixture. Plant extracts were mixed 1:1 with 100 pmol of internal standard (chrysin, MW = 254.2). Dihydroxybenzoic acid (DHB, 10 mg/mL) was used as the conventional matrix in the control MALDI-MS experiment. Before sample deposition, the substrate was briefly rinsed with HF to remove any residual SiO_2 layer. A 0.5-μL aliquot of analyte solution was spotted on the wafer afterward, and the surface was dried under vacuum to improve coating homogeneity. Samples were analyzed immediately. An Applied Biosystems Voyager STR MALDI-TOF mass spectrometer (Framingham, MA) was operated at an accelerating voltage of 20 kV in a reflector or linear mode as indicated in the text. The laser intensity used was varied to achieve optimum performance. At each location five laser shots were summed to yield one spectrum, and five spectra from different locations of each sample spot were averaged to reduce "hot"-spot variations. Three replicas of each sample were examined to calculate the standard deviation of the measurements. The signal-to-noise ratio of each MS peak was calculated automatically by the instrument software.

Scheme 1. Ordered Si Nanocavity Arrays Fabricated Using Nanosphere Lithography with Reactive Ion Etching (RIE)

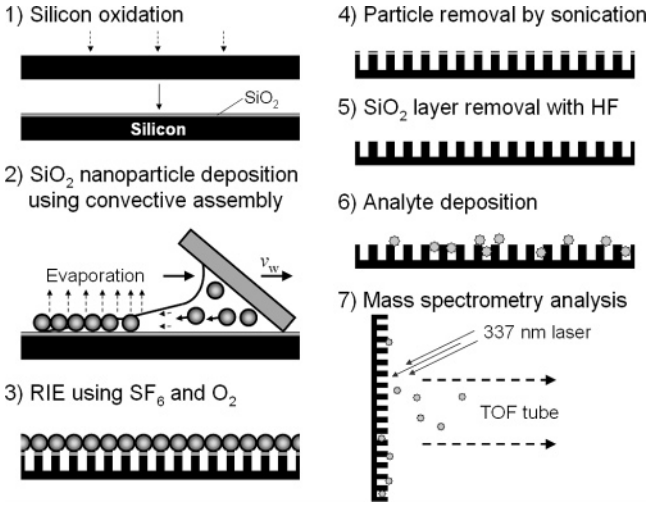

RESULTS AND DISCUSSION

Scheme 1 shows an overall design to fabricate ordered nanocavity arrays as SALDI substrates. (Note that, in further discussion, the term of "DIOS substrates" is used to refer to the substrates prepared using the anodic etching method specifically, whereas "SALDI substrates" are used for all other nonconventional matrix-based substrates, including our nanocavity arrays.) While this fabrication concept is generally applicable to a variety of materials, the success of low-resistivity Si wafers in DIOS makes it the preferred material in our experiments. In addition, the robustness of Si in laser irradiation, high surface affinity toward biomolecules, and ease of handling are also attractive for these proof-of-concept experiments.

For a consistent particle deposition, a thin layer of SiO_2 (3−5 nm) was generated atop the Si wafer to improve surface hydrophilicity. SiO_2 nanoparticles of 330 nm in diameter were deposited on the wafer subsequently using the coating apparatus described previously in the literature.[37,38,47] In this convective assembly process, it is known that the final crystal lattice formed depends critically on the volume of particle solution used, particle concentration, solvent evaporation rate, and the rate of meniscus withdrawal (controlled by the speed of the spreading plate). We found that 10−15 μL of SiO_2 particle suspension spread at a rate of 20−45 μm/s consistently produced close-packed SiO_2 nanoparticle arrays on the surface. The surface uniformity was inspected visually on the basis of the diffraction pattern from the crystal formation. Parts A and B of Figure 1 illustrate representative FE-SEM images of a monolayer of hexagonally packed SiO_2 nanoparticles assembled on a Si wafer at different scales. Note that local defects are observed due to the formation of crystal domains during the deposition. Considering the diameter of the

(47) Velev, O. D.; Lenhoff, A. M. *Curr. Opin. Colloid Interface Sci.* **2000**, *5*, 56−63.

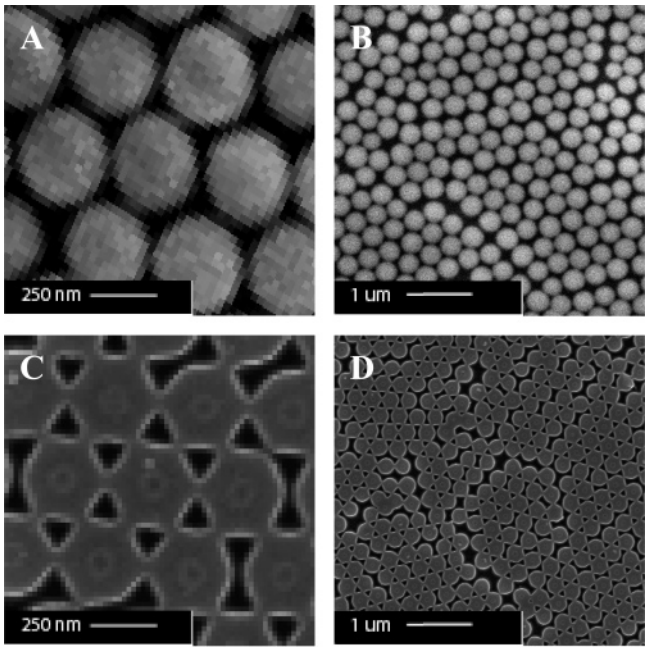

Figure 1. Monolayer of 330-nm SiO_2 nanoparticles spread on a Si surface using convective assembly. FE-SEM images of such Si wafer before (A, B) and after RIE, followed by the removal of nanoparticles with sonication (C, D). Images B and D are the overall surfaces, whereas A and C are the zoom-ins of the local hexagonal pattern.

laser beam used in our MS experiments was ~100 times larger than these defects, the interrogated substrate features were expected to be statistically consistent. Nevertheless, further optimization is underway to minimize the amount of the defects.

Following particle deposition, the wafer was directly loaded into a RIE chamber. A plasma mixture of SF_6 and O_2 was chosen to preferentially etch Si over SiO_2 to preserve the masked areas. Therefore, the portion of the Si wafer that was not shielded by the SiO_2 nanoparticles was selectively removed. Following RIE, the SiO_2 nanoparticles were removed through vigorous sonication, leaving only ordered cavities on the surface that can be clearly observed as triangle-shaped holes in the FE-SEM images (Figure 1C,D). Note that the posts left behind (the Si portions that were protected from the etching gas by SiO_2 nanoparticles) were hexagonal-shaped instead of circular, a combined result of scattered etching gas molecules off contoured SiO_2 surfaces and crystal orientation of the Si wafer used.

Mixtures of standard peptides of different molecular weights were used to examine the performance of these nanocavity arrays as SALDI substrates. Figure 2 shows representative MS spectra of two peptide mixtures detected. A smooth Si surface that had never been exposed to RIE was used as the control substrate. No signals were observed from such surface under the same experimental conditions, which eliminated the possibility of direct laser desorption of analytes. Small peptides such as Val-Met (MW = 248.1) and Ala-Leu-Ala-Leu (MW = 386.3) were clearly detected at spectral locations that are often overcrowded with conventional matrixes and matrix adduct peaks. The signal-to-noise (S/N) ratios of the detected peptides were comparable to those detected from

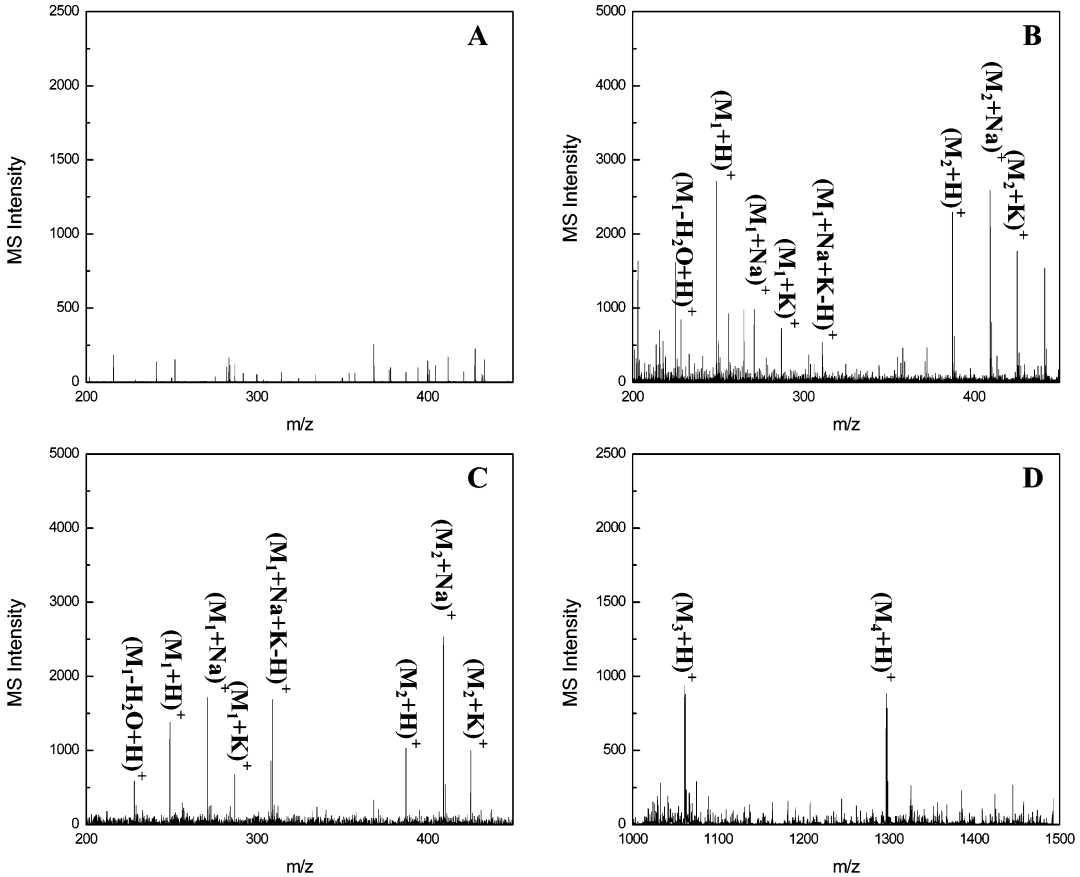

Figure 2. MS detection of a mixture of Val-Met (M_1) and Ala-Leu-Ala-Leu (M_2) on an unetched Si wafer (A), a DIOS substrate (B), and a surface with the nanocavity array (C). Panel D showed the detection of bradykinin (M_3) and angiotensin I (M_4) on the arrayed surface. The arrayed Si surface was treated for 1 min with RIE. The peaks corresponding to the peptides and their adducts assigned. MS spectra were collected in a reflector mode.

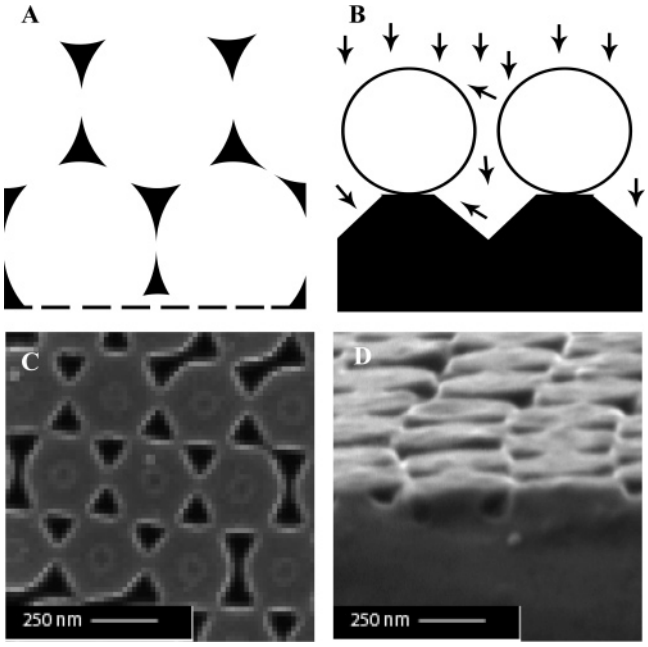

Figure 3. Schematic drawings of the top view (A) and the side view (B) of a SiO_2 nanoparticle-masked surface during RIE. The dotted line in panel A indicates the cross-sectioning position for the side-view scheme; the arrows in panel B represent etching molecules. Corresponding FE-SEM images are shown in panels C and D, respectively. The surface was prepared with 1-min etching.

conventional DIOS substrates, with slightly less background noise observed (Figure 2B,C). Detailed comparison on the sensitivity and reproducibility of these two substrates is currently underway. Larger peptides, bradykinin and angiotensin I, were also detected using a nanocavity array, although more background noise was observed due to the higher laser energy needed for desorption (Figure 2D).

Significantly increased surface roughness has been suggested as the main reason for the observed high desorption efficiency of DIOS substrates in the past.[10] Therefore, we prepared a series of substrates of different cavity geometries to examine the possible correlation of surface roughness to the observed MS signals. Theoretically speaking, the exact geometry of the cavities etched onto the surface is a function of the wafer crystal orientation, the geometry of the mask opening, and the duration of the etching. However, when spherical particles were used as the mask in RIE, an extensive energetic gaseous molecule bombardment on the mask particles occurs and causes the etching area to deviate from the geometry of mask opening (Figure 3B).[48] Indeed, we noticed that the features generated initially were smaller than the mask opening due to the gaseous etchants scattering off SiO_2 nanoparticle surfaces. Longer etching time allowed the etching molecules to diffuse or scatter into the gaps between the mask and the Si surface, leading to the removal of Si clusters underneath the particles and the generation of larger cavities. This nondirectional etching was also supported by detailed examination of the FE-SEM image of the 1-min etched surface. Small protruding Si residues were clearly observed at the contact points between particles and the surface (Figure 3C,D). These protruded features

(48) Coburn, J. W. *Plasma Etching and Reactive Ion Etching*; American Institute of Physics: New York, 1982.

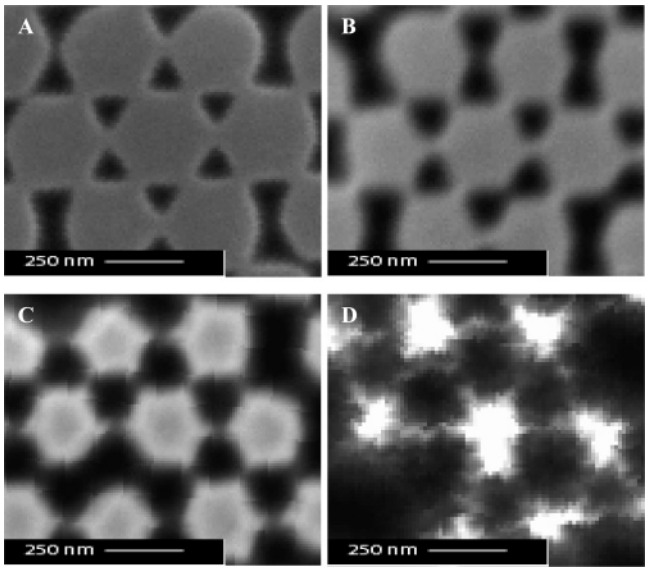

Figure 4. Top-down FE-SEM images of nanocavity Si surfaces etched for 0.5 (A), 1 (B), 1.5 (C), and 5 min (D). The images were adjusted to show the same magnification scale for comparison.

were believed to be the leftovers of Si underneath the mask particles, as the surrounding areas were shaved off by the scattered etching gas. Note that the lateral etching was at a much slower rate, as only a small portion of scattered gas molecules was able to reach the surface underneath the particles, whereas the majority of molecules were scattered toward different directions and were removed eventually with continuous vacuum pumping. Besides scattering-caused deviation the mixture of SF_6/O_2 etching gas also eroded away SiO_2 nanoparticles, albeit at a much slower rate (1:20 SiO_2 vs Si etching rate). Consequently, a larger opening area was exposed gradually with the continuous reduction of the mask size. Together, the combined result of etchant divergence and reduction of SiO_2 mask size was the observation of an increased in-plane cavity width with extended etching time (Figure 4A−D).

The etching time also affects the out-of-plane depth of the cavities formed. The cross-sections of the nanocavities showed the formation of tapered holes instead straight channels (Figure 3D). Again, the aforementioned etching gas divergence and mask losses probably are accountable for this observed geometry. The changes in the in-plane width and depth of the cavities formed at different conditions were plotted into a calibration curve, so appropriate experimental conditions can be estimated in order to obtain desired surface geometry in our later experiments (Supporting Information). While the roughness of the inner wall of the cavity was difficult to characterize with our current instrument, the FE-SEM image of the cross-sections of the cavities formed after short-period etchings showed relatively smooth edges and no apparent formation of nanochannels inside. However, the roughness of the inner wall of the cavity was expected to increase with extended etching times.

Figure 5 shows representative MS spectra of the mixture of Val-Met and Ala-Leu-Ala-Leu detected under similar conditions from the surfaces etched for 0.5, 1, 1.5, and 5 min. While absolute signal intensity was improved with increasing surface cavity sizes, the background noise also became more pronounced. The fragile Si skeleton network between residual posts was considered the

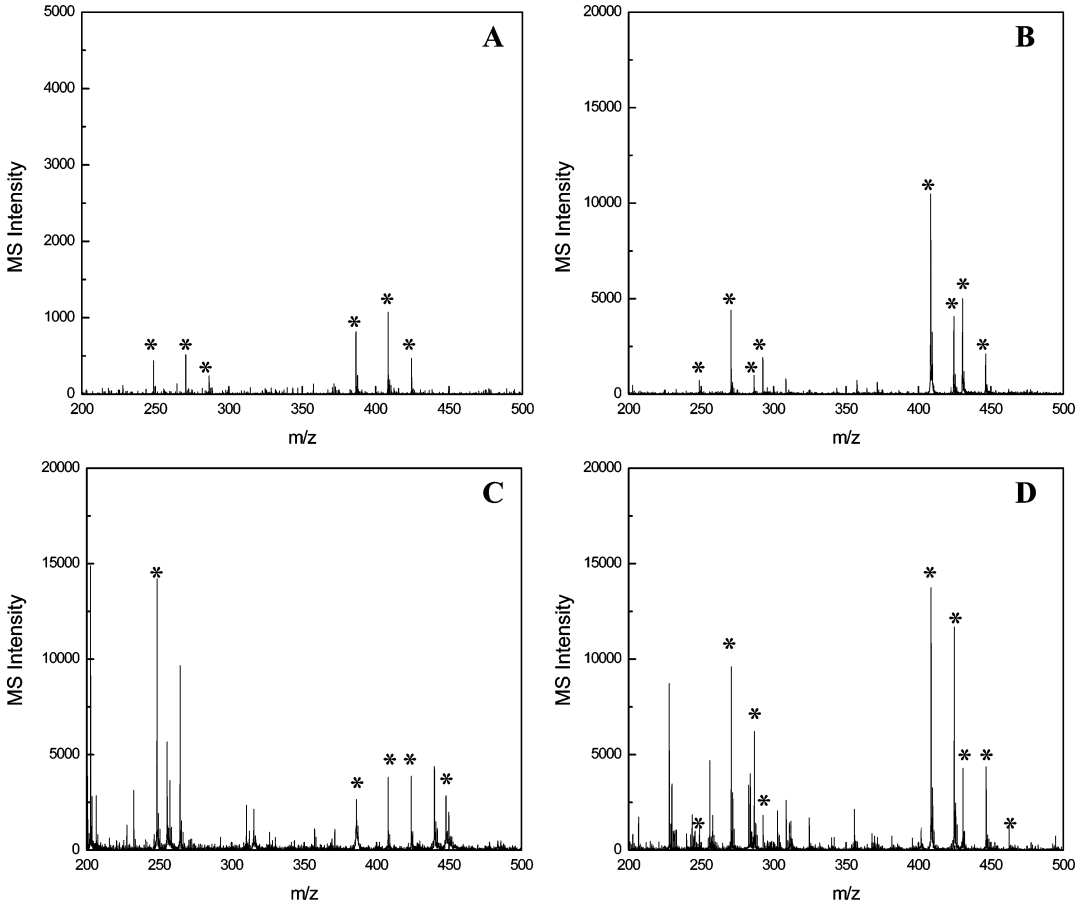

Figure 5. MS detection of Val-Met and Ala-Leu-Ala-Leu from nanocavity arrayed Si surfaces etched for 0.5 (A), 1 (B), 1.5 (C), and 5 min (D). Analytes were detected in a linear mode with similar laser intensities. Relevant MS peaks are labeled with asterisks.

main cause of the background noise in the form of Si clusters. As the cavity width and depth were changing concurrently, the percentage of the total surface area increased after each etching period was used to semiquantitatively characterize the impacts of surface roughness. The surface area was calculated on the basis of the measurement of cavity widths and depths (Supporting Information). It is worth pointing out that larger surface features (width or depth) do not translate automatically to a rougher surface, i.e., larger surface area. However, for the substrates we have studied, the surface areas calculated increase monotonically with the cavity sizes. The MS signal-to-noise ratios of each analyte and its adducts instead of their relative intensities were calculated to reduce the artifacts from the increased background noise of extensively etched surfaces. The results were plotted against the changes in the total surface areas in Figure 6. Decreased MS responses were observed initially with the increase of cavity sizes. This is consistent to what has been reported previously in the literature that smaller Si pores in DIOS often exhibit better MS performance.[10] It is important to point out that an absence of MS response from a smooth Si surface, i.e., zero increase of the surface area, was observed in the control experiment, which suggested an optimal surface roughness probably existed somewhere in between. We are currently working on methods to further reduce cavity sizes to study the corresponding MS behavior of the substrates in this region. Interestingly, with a further increase in the surface total area, a surprising recovering of MS intensity was later observed from heavily etched surfaces.

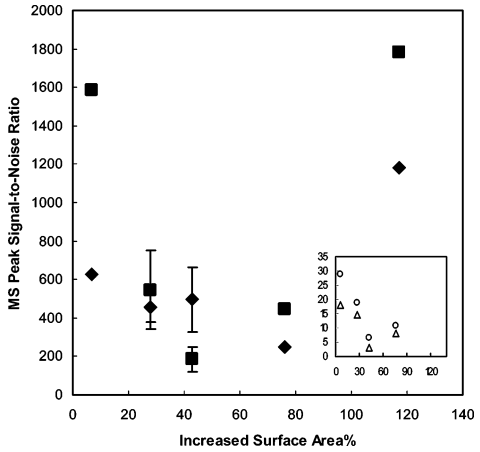

Figure 6. Signal-to-noise ratios of MS peaks plotted as a function of increased surface area percent after particle-masked RIE etching. Val-Met (◆), Ala-Leu-Ala-Leu (■), bradykinin (△), and angiotensin I (○) were used as the analytes. The error bars were calculated from three measurement replicas. See text for details in the calculation.

Note that while considerable error in the surface area calculation may exist due to the difficulty in accurate measurement of surface geometry, this later increase in MS responses was consistently observed from all four peptides examined.

On the basis of our experimental results and what have been reported in the literature, we speculate that the observed surface area-dependent phenomenon was a result of the interplay of

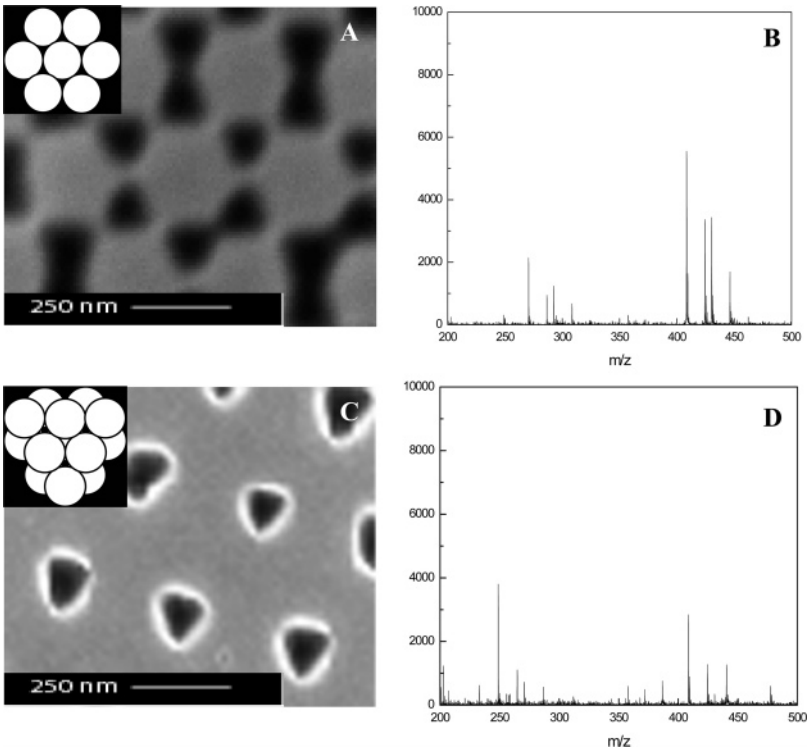

Figure 7. FE-SEM images of a nanocavity Si surface formed using a monolayer (A) or a bilayer (C) of SiO_2 beads as the mask. The insets show the schematic drawings of surface assembly. Corresponding MS spectra of the peptide mixture of Val-Met and Ala-Leu-Ala-Leu are shown as panels B and D, respectively. The etching time for the substrates used was carried out for 1 min. MS spectra were collected in a reflector mode.

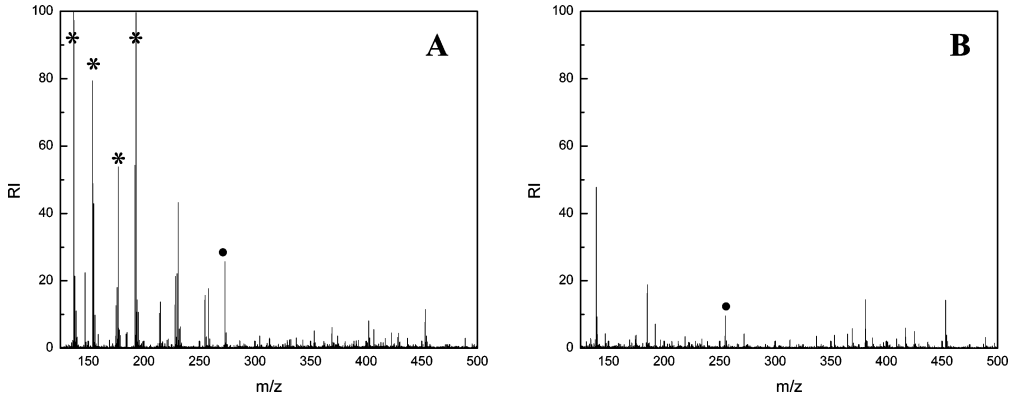

Figure 8. MALDI-MS detection of *Arabidopsis thaliana* root extracts using DHB as the conventional matrix (A) and SALDI-MS detection using nanocavity arrayed Si surface (B) of the same plant extract sample. Matrix peaks from DHB are labeled with asterisks. Internal standard is labeled with dots. MS spectra were collected in a reflector mode.

multiple attributors working collectively.[49−54] These attributors could be roughly divided into two categories: (1) those that promote analyte desorption/ionization at smaller surface features and (2) those support better MS responses from larger surface features. For example, the thermal conductivity of a Si roughened wafer is significantly smaller than a smoothed one.[50] An increase in the local temperature upon laser irradiation has been observed for surfaces with cavities. Subsequently, a more dramatic expansion of the entrapped gas inside those surface cavities is expected that could lead to a more efficient liberation of physically adhered analytes.[10,15] Intuitively, this heat-induced gas expansion is expected to be more pronounced for smaller cavities and becomes less significant with increasing cavity sizes. Another possible factor is related to the optical property of the surface: the strong ultraviolet absorption of porous Si surfaces indicates an electromagnetic (EM) interaction of the surface with the 337-nm laser irradiation source.[51,52] Known as the "lightening rod" phenomenon, a curvature-dependent EM field enhancement is expected to be more pronounced with smaller cavities.[15] On the other hand, a simple increase in the surface area accessible for analyte absorp-

(49) Hanley, L.; Kornienko, O.; Ada, E. T.; Fuoco, E. Trevor, J. L. *J. Mass Spectrom.* **1999**, *34*, 705−723.
(50) Shen, Q.; Toyoda, T. *J. Therm. Anal. Calorim.* **2002**, *69*, 1067−1073.
(51) Maly, P.; Trojanek, F.; Valenta, J.; Kohlova, V.; Banas, S.; Vacha, M.; Adamec, F.; Dian, J.; Hala, J.; Pelant, I. *J. Lumin.* **1994**, *60−61*, 441−444.
(52) Liu, H.; Fonseca, L. F.; Mahfoud, A.; Resto, O.; Weisz, S. Z. *Proc. SPIE-Int. Soc. Opt. Eng.* **2003**, *5061*, 149−155.
(53) Zhu, Y.; Zhang, L. D. *J. Phys.: Condens. Matter* **1999**, *11*, L491−L495.
(54) Shalaev, V. M. *Handbook of Nanostructured Materials and Nanotechnology*; Academic Press: New York, 2000.

tion has been recognized to enhance MS response with larger surface areas.[10] With more analytes exposed under the laser beam concurrently, an increase of MS response from substrates prepared with longer etching times is expected. We suspect that the surface thermal property and the EM coupling may be the key players for surfaces with smaller cavities that result in the observed decreased MS performance with increased surface area initially. The contribution from the increased surface area available for adsorption becomes more dominant with larger cavities, resulting in a later recovery of MS response. Increased surface roughness inside the cavities after an extended etching process may also be accountable to this later increase in signal. The existence of other substrate-related causes, such as analyte solvation and surface conductivity changes, are also acknowledged.[15,49] Combinatorially varying surface geometries to quantitate the individual contribution is underway.

Critical to the study of the EM coupling between neighboring cavities, surface cavity density also needs to be tunable besides aforementioned feature sizes. We therefore diluted cavity density by using a bilayer masking method. Specifically, by increasing the amount of the nanoparticles used in convective assembly, a second layer of particles was deposited atop the first layer, with each particle sat at the 3-fold hollow site of the first layer. Subsequent RIE produced a nanocavity pattern at half of the original cavity density on the surface (Figure 7A,C). On the basis of nanoparticle packing, hexagonal-shaped cavities were expected (Figure 7A,C insets). However, triangular-shaped ones were still observed instead. It may again be due to the scattered etching gas that preferably removed Si atoms along the lattice directions. With about half of the total surface area available for analyte adsorption but of similar cavity dimension, a decreased MS response was observed as expected (Figure 7B,D).

To examine the use of these nanocavity arrays in practical applications, *A. thaliana* root extracts were analyzed for their metabolite content in a proof-of-concept experiment.[55,56] It is not surprising to see that DHB as the conventional matrix used in the control MALDI-MS experiment clouded the detection of small molecules (Figure 8A), whereas arrayed Si surface exhibited much cleaner spectrum showing sample-related information (Figure 8B). Identification and quantitation of those biologically important peaks will be reported in a separate paper. It is clear, however, that the ordered nanocavity SALDI substrates can be used in small molecule profiling.

CONCLUSION

Arrayed Si nanocavity surface has been fabricated using a convective assembly coupled RIE process. Cavity width, depth, and intercavity spacing were varied to study MS desorption/ionization performance. Several possible causes were speculated to explain the observed correlation between surface features and the observed MS responses. But a more detailed study to quantitate the contribution of each factor is needed to unveil the key factors contributing to the SALDI phenomenon. These patterned nanocavity arrays of tunable features could find applications in reproducible metabolite profiling. The same surface fabrication concept can also be extended to various materials, such as carbon and metallic nanofeatures, to examine their performance as desorption and ionization media in a similar format.

ACKNOWLEDGMENT

The authors thank Dr. Ginger Yu and NCSU Nanofabrication Facility for the help with the RIE process. We also thank Drs. Wendy Boss and Imara Perera for their help on plant extract preparation.

SUPPORTING INFORMATION AVAILABLE

Surface cavity geometry measurements, cavity etching rates, and total pore surface area calculation (pdf). This material is available free of charge via the Internet at http://pubs.acs.org.

Received for review September 13, 2004. Accepted November 24, 2004.

AC048645V

(55) Fiehn, O.; Kopka, J.; Dormann, P.; Altmann, T.; Trethewey, R. N.; Willmitzer, L. *Nat. Biotechnol.* **2001**, *19*, 173−173.

(56) von Roepenack-Lahaye, E.; Degenkolb, T.; Zerjeski, M.; Franz, M.; Roth, U.; Wessjohann, L.; Schmidt, J.; Scheel, D.; Clemens, S. *Plant Physiol.* **2004**, *134*, 548−559.